

MS. HANAA DEIK (Orcid ID : 0000-0002-2658-7239)

DR. LARS REUNING (Orcid ID : 0000-0002-3796-2874)

Article type : Original Manuscript

The sedimentary record of Quaternary glacial to interglacial sea-level change on a subtropical carbonate ramp: Southwest Shelf of Australia

HANAA DEIK*, LARS REUNING†, MARGOT COURTILLAT‡, BENJAMIN PETRICK¶ and MARIA-ANGELA BASSETTI‡

*Geological Institute, RWTH Aachen University, Wüllnerstrasse2, 52062 Aachen, Germany (E-mail: hanaa.deik@rwth-aachen.de)

†Institute of Geosciences, CAU Kiel University, Ludewig-Meyn-Straße 10, 24118 Kiel, Germany

‡CEFREM UMR5110, University of Perpignan, 52 Avenue Paul Alduy 66860, Perpignan, France

¶Max Planck Institute for Chemistry, Climate Geochemistry Department, Hahn-Meitner-Weg 1, 55128 Mainz, Germany

Associate Editor – Tracy Frank

Short Title – Sedimentary record of Quaternary sea-level change, Southwest Shelf, Australia

This article has been accepted for publication and undergone full peer review but has not been through the copyediting, typesetting, pagination and proofreading process, which may lead to differences between this version and the [Version of Record](#). Please cite this article as [doi: 10.1111/SED.12793](https://doi.org/10.1111/SED.12793)

This article is protected by copyright. All rights reserved

ABSTRACT

In the last decades, the understanding of temperate carbonate systems has improved considerably, but their development over glacial–interglacial timescales is still understudied in comparison to their tropical counterparts. A key question is how do temperate carbonate platforms respond to high-amplitude, glacial–interglacial sea-level changes? Integrated Ocean Drilling Program Site U1460 was drilled at the uppermost slope of the Southwest Shelf of Australia at the transition between the subtropical Carnarvon Ramp and the warm–temperate Rottneest Shelf. The origin and composition of the sediments in the upper 25 m below seafloor at Site U1460 were investigated using X-ray diffraction, scanning electron, and light microscopy. The Middle Pleistocene to Holocene sequence at Integrated Ocean Drilling Program Site U1460 contains a record of sea-level controlled sedimentary cycles. Carbonate sediments deposited during interglacial sea-level highstands (Marine Isotope Stages 1, 5, most of 7, 9 and 11) are mainly fine-grained (<63 μm) and dominated by low-Mg calcite from pelagic bioclasts such as planktic foraminifera. The glacial lowstand intervals (Marine Isotope Stages 2 to 4, 6, 8, 7d, 10 and 12), instead are coarser-grained and relatively rich in aragonite and high-Mg calcite from neritic bioclasts, such as bryozoans. These changes in texture, mineralogy and composition are best explained by the deposition of neritic bioclasts closer to the shelf edge during glacial sea-level lowstands. During early transgression, reworking of bioclast-rich coastal dune deposits likely leads to transport and redeposition of neritic clasts on the upper slope. In contrast, dominantly pelagic sediments characterize deposition at the platform edge during interglacial highstands. These results highlight regional differences in the response of temperate carbonate systems to sea-level change: A previously published model developed for early Pleistocene temperate carbonates from the Great Australian Bight indicates that shelfal material was exported to the upper slope during sea-level highstands. It is argued that this difference is related to the change in duration and amplitude of glacial-interglacial sea-level cycles before and after the Mid-Pleistocene transition.

KEYWORDS Aragonite, IODP Expedition 356, International Ocean Discovery Program, Pleistocene, sedimentary cycles, temperate carbonates.

INTRODUCTION

Up to one third of all carbonate produced on continental shelves today comes from subtropical (James *et al.*, 1999) and temperate environments (James, 1997). Such deposits provide important modern analogues for many geologically ancient carbonate deposits (Nelson, 1988; James, 1997; Pedley & Carannante, 2006; Ryan *et al.*, 2008). Much of what is known about these carbonate systems has been learned from the study of modern seafloor sediments, with the southern and western Australian Shelves serving as key locations for warm–temperate carbonate settings (Collins *et al.*, 1993; James *et al.*, 1999; James & Bone, 2011). However, the accumulation rate on the southern Australian Shelf is low since most of the sediments are transported offshore by vigorous swells and storms (James *et al.*, 1994). Over much of the inner shelf this results in patchy sediment cover of palimpsest carbonates of Late Pleistocene to Holocene age (James *et al.*, 1994; Ryan *et al.*, 2008). On the outer shelf and slope sediment accumulation has been nearly continuous during the Quaternary (Feary *et al.*, 2000; Hine *et al.*, 2004; Deik *et al.*, 2019). These deposits provide an important archive for the response of the carbonate system to the high amplitude, glacial to interglacial, sea-level fluctuations of the Middle Pleistocene to Holocene (Andres & McKenzie, 2002; Hine *et al.*, 2002; Saxena & Betzler, 2003; Betzler *et al.*, 2005; Deik *et al.*, 2019).

Despite the progress in understanding of subtropical and temperate carbonate systems, they remain considerably less well studied compared to their tropical counterparts. For example, the widely used ‘highstand shedding’ concept predicts that carbonate production on flat-topped, tropical platforms and distally steepened ramps peaks during interglacial sea-level highstand when the inner platform is flooded (Schlager *et al.*, 1994). Because accommodation space is limited in the inner platform, the produced aragonite mud is transported into deeper water where it mixes with calcite from pelagic sources. This concept is underpinned by data from several tropical carbonate platforms showing higher aragonite and high-Mg calcite (HMC) content in slope sediments during interglacial times (Paul *et al.*, 2012; Eberli, 2013). The response of subtropical and temperate continental shelf systems to glacial–interglacial sea-level change is much less well understood. Two different models have been developed based on evidence from the Great Australian Bight (GAB). One model proposes that the wide warm–temperate carbonate platform of the Great Australian Bight (GAB) responds to sea-level change in a similar manner to tropical systems. In this model, the amount of material exported from the shallow shelf to the slope increases with the shelf area flooded during sea-level rise and highstand (Betzler *et al.*, 2005). The alternative model emphasizes increased export of shallow shelf sediments to the slope during sea-level lowstands, when the shelves are narrower and the high-energy zones closer to the shelf edge (James *et al.*, 1997; James & Bone, 2011). It is essential to study other temperate carbonate platforms outside the GAB, to test which of the two models can be applied more widely.

To investigate sedimentary processes in subtropical to temperate sediments deposited during high-amplitude, glacial-interglacial sea-level fluctuations, data from the western Australian Shelf is presented. The upper 25 m below seafloor (CSF-A) of core at Integrated Ocean Drilling Program (IODP) Site U1460, drilled on the upper slope during IODP Expedition 356 (Gallagher *et al.*, 2017), contains a nearly complete record of carbonate sedimentation from the Middle Pleistocene to the Holocene. The mineralogy, texture and composition of the sediment was analysed using X-ray diffraction, a scanning electron microscope equipped with an energy-dispersive X-ray spectrometer, light microscopy (Olympus BH-2; Olympus Corporation, Tokyo, Japan) and grain-size analysis. The results were compared with existing age models to characterize sea-level highstand and lowstand deposits and develop a conceptual model for their formation.

GEOLOGICAL SETTING

The environment of the western continental margin of Australia in the eastern Indian Ocean is transitional between warm–temperate and tropical carbonate settings. It comprises the warm–temperate Rottneest Shelf in the south (south of 28°S) and the subtropical Carnarvon Ramp in the north (22 to 28°S). Reef growth at this relatively high latitude is facilitated by the Leeuwin Current flowing southward along the west coast of Australia; it is a current of low salinity, warm surface water, sourced from the Indonesian Throughflow (ITF) (Cresswell *et al.*, 1989). During glacials the Leeuwin Current is believed to be considerably weakened (Spooner *et al.*, 2011; Petrick *et al.* 2019). The Houtman Abrolhos Reef complex, which contains the southernmost major tropical reef in the Indian Ocean (28 to 29.5°S), straddles the boundary between the Carnarvon Ramp and the Rottneest Shelf (Fig. 1). For both areas James *et al.* (1999) described the shelf morphology and facies distribution on the modern seafloor. The modern-shelf sediments are characterized by a distinct cool-water composition (Nelson, 1988), but with subtropical attributes (James *et al.*, 1997). The skeletal assemblage is dominated by coralline algae, bryozoans, molluscs (scaphopods, bivalves and gastropods) and foraminifera (James *et al.*, 1997). The main difference from typical cool-water deposits is the presence of scattered zooxanthellate corals and large, symbiont-bearing foraminifera (James *et al.*, 1999; Collins *et al.*, 2014). Skeletons of serpulid worms, echinoids, azooxanthellate corals and sponge spicules are of local importance. The calcareous green algae *Halimeda* grows locally on the shelf and ramp but is poorly calcified and therefore generally does not contribute to the sediment outside Shark Bay. The seafloor above *ca* 50 to 60 m is subject to constant reworking and abrasion by waves, while the swell wave base is close to 100 m, leading to a lack of mud deposition above this depth (James *et al.*, 1999).

The Carnarvon Ramp comprises the Ningaloo Reef and hypersaline Shark Bay on the inner ramp (Fig. 1A and B). The mid-ramp is euphotic, with relatively little calcareous benthos and low numbers of

bryozoans, coralline algae and larger foraminifera, but is dominated by relict or stranded foraminiferal-dominated sand. The outer ramp is pelagic in character, covered by planktic foraminiferal sand or spiculitic mud. The outflow of highly saline waters from Shark Bay leads to periodic downwelling of relatively warm and saline waters across the ramp (James *et al.*, 1999; Collins *et al.*, 2014). Between 27° and 28°N the Carnarvon Ramp transitions into the Rottnest Shelf (Fig. 1A and B). The Rottnest Shelf is flat-topped, with a wave-swept, 30 to 70 m deep inner-shelf plain characterized by rhodolith pavements, bryozoans, sponges and abraded sediments (Fig. 1C). An incipient rim formed by a linear ridge system covered by rhodolith gravel separates the inner shelf from the subphotic outer shelf that is dominated by bryozoans, benthic foraminifera and molluscs (Fig. 1). This ridge system likely represents a stranded coastal dune system that formed when sea-level was considerably lower than today during Marine Isotope Stages (MIS) 3/4 (Brooke *et al.*, 2010, 2014). The upper slope contains fine sand and silt of bryozoan fragments, sponge spicules and planktic foraminifera (James *et al.*, 1999). Essentially, this facies extends south to *ca* 34°S on the shelf offshore Cape Leeuwin (Collins, 1988). The eastward decreasing influence of the Leeuwin Current is reflected in the impoverished fauna of warm-water, benthic foraminifera east of Cape Leeuwin. However, the benthic foraminifera *Amphisoris* (*Marginopora*) occur commonly together with non-calcified green algae and scattered zooxanthellate corals along the inner Albany Shelf (Li *et al.*, 1999). Subtropical faunal elements are missing further to the east in the Great Australian Bight but were present, for example, during the early Pleistocene (Gelasian) and interglacial MIS 5e (James & Bone, 2007, 2011).

The IODP Site U1460 was drilled during IODP Expedition 356 on the Southwest Shelf of Australia (27°22.4867'S and 112°55.4265'E; Fig. 1). The site is situated on the uppermost slope in a water depth of *ca* 214 m (Fig. 1C). It is situated north of the Houtman Abrolhos reef complex, at the transition between the Carnarvon Ramp in the north and the Rottnest Shelf towards the south (Fig. 1A and B). This transition zone shows a mixture of morphological and facies characteristics of both regions.

Cores were recovered from two boreholes (A and B) at IODP Site U1460 (Fig. 2) and drilled with the long hydraulic piston core (HLAPC) system. The sediment recovery in both holes was generally excellent (97 to 98%), with minor gaps between cores resulting from the HLAPC system (Fig. 2). The shipboard correlation between holes is based on gamma-ray data. The correlation was not detailed enough to produce a continuous composite depth scale, but generally cores in both holes are at similar depth (Fig. 2; Gallagher *et al.*, 2017). Coring of gravel-rich grainstone to floatstone layers produced minor gaps and intervals with reduced core integrity leading to reduced confidence in the correlations between holes (Fig. 2; Gallagher *et al.*, 2017).

The sediments recovered at IODP Site U1460 consists of two lithostratigraphic units (I and II), with Unit I subdivided into three subunits (Ia, Ib and Ic) (Gallagher *et al.*, 2017). The studied interval (0 to 25 m CSF-A) is entirely from subunit Ia (Fig. 2A to I; 0 to 44.94 m CSF-A).

Subunit Ia is characterized by beige to greenish-grey skeletal packstones (Gallagher *et al.*, 2017). Based on visual estimates, the skeletal assemblage is dominated by planktic foraminifera, fragments of bivalves and gastropods (including pteropods), bryozoans, echinoids, and some azooxanthellate corals, intraclasts and peloids (Fig. 3A to I; Deik *et al.*, 2019). The packstones are interbedded with skeletal wackestones, mudstones and macrofossil rich grainstones to floatstones (Fig. 2). The silt to sand size fraction in the grainstones to floatstones consists predominantly of bryozoan fragments, the rest is comprised of variable proportions of foraminifera, molluscs, serpulids, echinoids, and minor amounts of azooxanthellate corals, ascidians spicules and scaphopods. The gravel fraction has a similar composition but also contains many skeletal intraclasts. Faecal pellets (Fig. 3) and quartz grains are generally absent in all of these coarse-grained intercalations (Deik *et al.*, 2019).

According to the interpretation of Deik *et al.* (2019) the composition of mud to packstones in Subunit Ia (Fig. 2) is very similar to the planktic sand and silt facies (P2; James *et al.*, 1999) on the present seafloor (Fig. 1). In contrast, the coarser-grained intercalations of grainstones to floatstones (Fig. 2) are similar in composition to the bryozoan skeletal sand facies (Hole B; James *et al.*, 1999) on the modern-day seafloor (Fig. 1).

AGE MODEL

Based on the shipboard biostratigraphy (Gallagher *et al.*, 2017) the cores U1460B-1F to 7F (0 to 25 m CSF- A) represent the last *ca* 450 kyr (Fig. 2). The inner shelf in the study area is up to 70 m deep (Fig. 1). For the studied time interval, global sea-level fell below this level during MIS stages 2 to 4, 6, 8, 10 and 12 and substage MIS 7d. These stages will be referred to as times of glacial sea-level lowstand in this study. During MIS 1, 5, 9, 11 and most of 7 the shelf plain was most likely partially to completely flooded. Those MIS will be referred to as times of interglacial sea-level highstands. Further offshore western Australia, the aforementioned glacials were characterized by a weakening of the Leeuwin Current and several degrees colder sea-surface temperatures compared to times of interglacial sea-level highstands (Spooner *et al.*, 2011).

Two previously published age models are available for IODP Site U1460, which are based on temperature-dependent proxy records (Figs 2 and 3). Petrick *et al.* (2019) used the biomarker TEX₈₆ record tuned to the benthic isotope stack LR04 (Lisiecki & Raymo, 2005) to construct an age model for Hole B. The absolute temperatures of this reconstruction have a two-sigma standard deviation of ± 5 to 6°C, but

relative changes in temperature are well constrained and reflect Leeuwin current dynamics (Petrick *et al.*, 2019). Alternatively, Courtillat (2019) used a $\delta^{18}\text{O}$ record of the planktic foraminifer *Globigerinoides ruber* in combination with ^{14}C ages and *G. menardii* complex abundance data to construct an age model mainly based on samples from Hole A (Fig. 2). Generally, both age models show a good match over the studied interval (Fig. 2). A discrepancy between the age models exists for the time interval MIS 6 to 7, although the shape of the two temperature records is actually quite similar in this depth interval (Fig. 2). The generally warm MIS 7 contains the substage 7d (Fig. 2I) that experienced very cold temperatures at a global scale that are unusual within an interglacial (Pahnke *et al.*, 2003). This substage also stands out in climate proxy records from western Australia as a cold and arid time interval (Spooner *et al.*, 2011; Stuut *et al.*, 2014). The presence of this cold substage likely explains the difficulty in assigning an absolute age to this interval. However, the aim of the study presented here was to discriminate times of sea-level lowstands from highstands in the core, rather than to assign absolute ages. With few exceptions, glacial (interglacial) conditions are therefore interpreted for the intervals that were unanimously identified as cold (warm) intervals in both age models (Fig. 2). The MIS 1/2 boundary is defined following Courtillat (2019), who constrained its position using ^{14}C ages. The MIS 10/11 boundary is placed at the base of a grainstone/floatstone layer in both age models. The small depth offset of these two coarse-grained layers between holes likely results from small core gaps in Hole U1460B. The present study places the boundary of MIS 11/12 at 23.17 m CSF-A according to the age model of Courtillat (2019), since a core gap in Hole B prevented sampling of this interval for biomarker analysis (Petrick *et al.*, 2019). Overall, the combination of the two proxy records enables attribution of most intervals to glacial or interglacial conditions with high confidence. The linear sedimentation rate for the entire interval is 5.8 cm/kyr.

METHODS

X-ray diffraction (XRD) analysis of 56 bulk samples from IODP Hole U1460B was used to quantify mineralogy. Six of these analyses were reported in Deik *et al.* (2019). In addition to the bulk samples, the mineralogy of the <34 μm and 34 to 63 μm fraction of those six samples was analysed. All XRD samples were oven-dried, ground and mounted on sample holders. The measurements were conducted using a Siemens D5000 X-ray diffractometer over an angle field of 60° (4° to 64°) with a step size of 0.02° per second [Bruker (Siemens), Billerica, MA, USA]. Identification and quantification of different mineral phases was achieved with the software DIFFRAC EVA (ver. 8.0) by Bruker. The relative abundance of mineral phases was determined using the I/I corundum values from the International Centre for Diffraction Data database. If quartz was present, it was used as an internal standard, and the measured quartz major peak d-spacing was adjusted to align with the known quartz major peak d-spacing. All other mineral phases

were adjusted accordingly. Where dolomite or high-Mg calcite (HMC, >4 mol % MgCO₃) was present in a sample, their MgCO₃ content was calculated based on the d-value of the [104] peak (Lumsden, 1979).

A total of 84 samples from IODP Holes U1460A and U1460B were wet sieved through a 63 µm sieve, and the retained sand fraction (>63 µm) for each sample was weighed and reported as % sand fraction (Fig. 2). The >63 µm fraction was dry sieved through a 150 µm mesh. The abundance of planktic foraminifera and bryozoans was counted in the >150 µm fraction under a binocular microscope to quantify the contribution from pelagic versus neritic sources. Scanning electron microscopy (SEM, Zeiss Supra 55, Carl Zeiss AG, Oberkochen, Germany) was used to further analyse the bulk sediment. The mineralogy of grains was confirmed by elemental analysis (Sr, S, Fe and Mg) with an energy-dispersive X-ray spectrometer (EDX Xmax 150; Oxford Instruments, Abingdon, UK). All samples were carbon coated prior to analysis. Six thin sections were prepared for petrographic analysis (Olympus BH-2) of the bulk sediment.

RESULTS

Mineralogy and grain size

The upper 25 m CSF-A at the IODP Site U1460 is generally dominated by sand-sized grains. Gravel is concentrated in certain grain to floatstone intervals, for example, around 17 m CSF-A (Fig. 2). The coarse size fraction (>63 µm) in average contributes about two-thirds to the sediment, while less than 5% of all samples are dominated by the fine fraction (Fig. 2).

The abundance of planktic foraminifera shows high amplitude fluctuations, with the highest values in intervals that are dominated by low-Mg calcite (LMC) and smaller grain sizes (Figs 3A to I and 4A to F). The highest peaks in bryozoan abundance occur in coarser-grained, aragonite-rich and high-Mg calcite-rich intervals (Fig. 3) with lower planktic foraminiferal concentrations. Intervals that are rich in bryozoans are also characterized by other neritic skeletal components such as bivalves, gastropods, worm tubes (Fig. 4A and B) and echinoderms. Benthic foraminifera (Fig. 4D) and azooxanthellate corals indiscriminately occur in intervals with high and low LMC contents. Peloids typically occur in LMC-rich, fine-grained intervals (Figs 3 and 4C). Ascidian spicules (Fig. 4E), sponge spicules and coccolith plates are important components in the fine fraction (<63 µm).

The carbonate content in the selected interval varies between 57% and 100%. The average carbonate content of the sediment is *ca* 91%, with 43% low-Mg calcite, 23% aragonite, 21% high-Mg calcite (HMC) and 4% dolomite (Fig. 2). The siliciclastic minerals plagioclase feldspar and quartz in total

contribute *ca* 9% to the sediment (Fig. 2). Quartz is present in almost all samples and its content varies between 0% and 11%, with an average of 4%. Based on six analysed samples, quartz content is higher in the 34 to 63 μm compared to the bulk and the <34 μm size fraction, with an average of about 9%, 5% and 3%, respectively (Table 1). Feldspar abundance shows an average value of 5% but exhibits a maximum of about 34% concentrated at a depth of around 19 m CSF-A (Fig. 2). Feldspar grain size typically ranges from silt to fine sand. Celestite (SrSO_4) was detected in only four samples and its content ranges between 3% and 11%.

The average aragonite content of the carbonate fraction is 25% but decreases from 37% at the top to 17% at the base of the analysed section (to *ca* 25 m CSF-A; Fig. 2). In the six analysed samples, aragonite content is higher in the 34 to 63 μm compare to the bulk and the fraction <34 μm fraction, with an average of about 34%, 25% and 23%, respectively (Table 1). However, one of the highest aragonite peaks occurs in the gravel-rich floatstone layer at around 17 m (Figs 2 and 4B), where the silt fraction is a very minor component (Fig. 2). Aragonite therefore seems to be concentrated on one hand in the coarse silt and on the other hand in the coarse sand to gravel fraction. The main aragonite producers in the sand fraction (>63 μm) are gastropods, bivalves, cheilostome bryozoans and some azooxanthellate corals (Fig. 4). Ascidian spicules contribute aragonite to the 34 to 63 μm fraction (Fig. 4E).

The HMC content in the carbonate fraction varies between 0% and 44%, with a mean of 23%. The HMC content shows stronger fluctuations compared to aragonite and a general decrease with depth. HMC is with 17% slightly less abundant in the finest grain size fraction (<34 μm) compared to the 34 to 63 μm (21%) and bulk (19%) fraction (Table 1). The MgCO_3 in HMC varies between 8% and 16 mol%, with a mean of 12%. Most of the HMC therefore is in a range that is sometimes referred to as intermediate-Mg calcite (IMC; 4 to 12 mol %; O'Connell & James, 2015). Less than one-third of all HMC samples actually have Mg values higher than 12%, and half of those occur in a depth shallower than *ca* 5 m CSF-A. HMC is mainly produced by echinoderms, benthic foraminifera such as miliolids and some serpulid worms (Fig. 4). Additionally, HMC occurs occasionally as cement.

Dolomite occurs below a depth of about 5 m CSF-A and its abundance is negatively correlated with aragonite content and HMC (Figs 2 and 3). The highest dolomite concentration is observed in the very fine fraction (<34 μm), with a mean of 5% compare to a mean of 4% and 3% in the 34 to 63 μm and bulk fraction, respectively (Table 1). The concentration of dolomite in the finest fraction is consistent with SEM observations; the euhedral rhombic dolomite crystals range in size from 5 to 20 μm (Fig. 4F), and occur in inter-particle and intra-particle pores similar to those described by (Rivers *et al.*, 2012). Unambiguous replacement of other carbonate phases by dolomite has not been observed, although sporadically dolomite crystals seem to engulf calcite grains (Fig. 4F). Therefore, they are interpreted to have formed as cement

phase. Detrital dolomites, characterized by signs of abrasion or weathering (Bone *et al.*, 1992; James *et al.*, 1994; Radwan *et al.*, 2018) are absent.

The dolomite is Ca-rich with calculated MgCO_3 contents ranging between 41 to 46 mol % (mean of 43 mol %) based on XRD, but no clear depth related trend. EDS measurements of individual dolomite crystals confirm the calculated MgCO_3 contents but show a somewhat higher variation from 32 to 45 mol %. It was not possible to identify the presence or absence of 'ordering' reflections for dolomite in the XRD spectra, due to the generally relatively low peak heights. It is therefore unclear whether the observed rhombohedral Ca-Mg carbonate should be specified as unordered dolomite (*sensu* Kaczmarek & Sibley, 2011) or ordered dolomite. Additional, more detailed information on the results is given in the Supplementary Tables S1 to S6.

DISCUSSION

Glacial–interglacial cycles

There is a strong control of glacial to interglacial sea-level on the sediment record (Figs 2, 3 and 5). During glacial sea-level lowstands (including MIS 2 to 4, 6, 8, 10, 12 and possibly 7d) the sediment is characterized by relatively high HMC and aragonite contents (Fig. 2). The sediment is coarser-grained and neritic components such as bryozoan fragments are more abundant (Figs 3 and 4). The intervals are poor in siliciclastics with quartz as the only significant non-carbonate phase. In contrast, intervals deposited during interglacial sea-level highstands (MIS 1, 5, most of 7, 9 and 11) contain more LMC, are finer-grained and show higher concentrations of pelagic material, such as planktic foraminifera (Figs 3 and 4). Dolomite is also enriched in interglacial highstand deposits. Detrital dolomite crystals showing variable degrees of rounding are a minor but recurring component on parts of the Eucla and Lacedpede shelves (Bone *et al.*, 1992; James *et al.*, 1994). They are mainly derived from the erosion of Cenozoic sediments (James & Bone, 2011). These detrital dolomites are often overgrown by a late dolomite cement that formed directly beneath the modern seafloor (Bone *et al.*, 1992). Dolomite crystals at IODP Site U1460 are always euhedral (Fig. 4F) and show no signs of abrasion. They probably formed preferentially in highstand sediments during early burial, likely favoured by the oxidation of organic matter as described by Swart & Melim (2000).

The siliciclastic content in interglacial intervals is higher and plagioclase feldspar is more abundant than quartz (Figs 2 and 3). Siliciclastic detrital grains on the modern-day Carnarvon Ramp are deposited in the coastal zone close to, for example the Murchison River mouth, where locally, they can contribute up to 40% of the sediment (James *et al.*, 1999). At IODP Site U1460, glacial intervals contain only quartz, while

interglacial intervals have a higher siliciclastic content consisting of silt to fine sand sized quartz and feldspar. Glacial to interglacial climate variability is shown by surface water temperature changes with an amplitude of 3 to 5°C (Fig. 2; Petrick *et al.*, 2019). It is also well-known that glacial intervals in western Australia were more arid (Rivers *et al.*, 2009) and windy compared to the interglacials (Stuut *et al.*, 2014; Hallenberger *et al.*, 2019; Petrick *et al.*, 2019). Wind-transported quartz was deposited offshore during the arid glacials (Stuut *et al.*, 2014), while other siliciclastic phases including feldspar indicate a more fluvial origin during more humid interglacials (Groeneveld *et al.*, 2017; Hallenberger *et al.*, 2019; Petrick *et al.*, 2019). The siliciclastic fraction at IODP Site U1460 therefore reflects the climatic variability of the late Middle Pleistocene to Holocene in Western Australia.

Could the increased wind strength also have contributed to the transport of relict carbonate grains to the shelf edge and slope during glacial sea-level lowstands? Detailed investigations by Nichol & Brook (2011) and Brook *et al.* (2014) have shown that relict skeletal grains were reworked into dunes on the exposed western Australian shelf during glacial sea-level lowstands. The ridge in the current study area that parallels the shelf break in a water depth of *ca* 60 m (Fig. 1) likely formed as such a coastal dune system during MIS 3/4 (Brook *et al.*, 2014). However, dune morphology and orientation of large-scale dune foresets further south on the Rottneest Shelf indicate that the dominant wind transport was directed onshore. It therefore seems likely that the aeolian transport of relict grains from the exposed shelf to the shelf edge during glacial sea-level lowstands was possible but likely limited due to the prevailing onshore winds.

The carbonate sediment on the modern, open to incipiently rimmed shelf is relatively coarse-grained bioclastic sand and gravel (Fig. 1; James *et al.*, 1999). The mud fraction is constantly winnowed by high-energy wave and swell abrasion from the shelf and deposited on to the outer ramp and slope (Fig. 5; James *et al.*, 1999), a mechanism very similar to the ‘shaved shelf’ proposed for the Great Australian Bight (GAB; James *et al.*, 1994). The skeletal assemblage on the shelf is dominated by coralline algae, bryozoans, molluscs (scaphopods, bivalves and gastropods) and foraminifera including large, symbiont-bearing foraminifera (Figs 1 and 5A to C; James *et al.*, 1999). The upper slope contains fine sand and silt consisting of sponge spicules and mainly calcitic bryozoan fragments, planktic foraminifera and nannofossils (James *et al.*, 1999; Collins *et al.*, 2014). Aragonitic components, such as pteropods and ascidian spicules never contribute more than 10% to the modern seafloor sediments at the outer ramp and slope (Fig. 5; James *et al.*, 1999). This difference in the depositional regime and skeletal assemblage between the shelf and slope results in coarser-grained, relative HMC-rich and aragonite-rich shelf sediments grading into fine-grained, more LMC-rich sediments on the slope (Fig. 5).

In the upper 25 m CSF-A at IODP Site U1460, relative HMC-rich and aragonite-rich, coarser-grained, neritic skeletal grain dominated glacial intervals alternate with finer-grained, LMC-rich, pelagic

dominated, interglacial intervals (Figs 2 to 5). This pattern is interpreted as reflecting a higher proportion of shelf-derived components in glacial deposits, whereas interglacial deposits are dominated by LMC-rich pelagic sediments. This pattern is ubiquitous throughout the studied interval (Fig. 5A and B), highlighted by variations of abundance of analysed components such as bryozoans and planktic foraminifera (Fig. 3).

Similar patterns have been recognized in the GAB (Saxena & Betzler, 2003; Betzler *et al.*, 2005); however the interpreted relationship to sea-level is reversed. Saxena & Betzler, (2003) and Betzler *et al.* (2005) analysed mainly early Pleistocene (Calabrian) intervals of several ODP sites on the upper slope of the Eucla Shelf. One of the sites (1129) is located closest to the shelf edge in a water depth of *ca* 200 m, nearly identical to IODP Site U1460. Those authors postulated that interglacial sea-level highstand deposits on the slope are dominated by relatively coarse-grained, aragonite-rich and HMC-rich bioclasts including bryozoan debris. In contrast, lowstand deposits were micritic, low-Mg calcite-rich sediments. Saxena & Betzler, (2003) and Betzler *et al.* (2005) concluded that HMC and aragonite-rich bioclasts were formed on the shallow, flooded shelf and exported to the slope during transgression and sea-level highstands. According to this model, the amount of material exported from the shelf to the slope increases with the shelf area flooded during sea-level rise and highstand, similar to the 'highstand shedding' concept developed for tropical platforms.

In contrast, other authors have emphasized the importance of redeposition events during glacial sea-level lowstand and early transgression, transporting coarser sediments from the relatively deep carbonate factory on the shelf to the slope, whereas highstands would be dominated by finer-grained, pelagic LMC sediments (Nelson *et al.*, 1982; Boreen & James, 1993; James, 1997; Passlow, 1997; James & Bone, 2011). Similarly, Puga-Bernabéu & Betzler (2008) relate HMC-bioclast rich intervals at the upper slope of the Pleistocene carbonate ramp of the GAB to the late sea-level fall and/or glacial sea-level lowstands. This increase in ramp sediment supply to the slope is interpreted to be a response to reworking by bottom currents. More pelagic LMC-rich intervals in contrast are related to interglacial sea-level highstands (Puga-Bernabéu & Betzler, 2008).

Results from the upper slope IODP Site U1460 from the Carnarvon Ramp (IODP Site U1460) indicate deposition of shelf derived, coarser-grained, HMC-rich and aragonite-rich bioclasts on the present-day upper slope during glacial sea-level lowstands (Figs 2 and 3). During sea-level lowstands, the zone of shelfal sediment production shifted towards the platform edge and therefore also closer to IODP Site U1460 (Fig. 5C). During sea-level minima, such as during MIS 2, the site would likely have situated above the swell wave base, leading to winnowing of the finer fraction (Deik *et al.*, 2019; Fig. 5C).

It is possible that initial flooding of the shelf during the post-glacial early sea level rise led to a pulse of shelfal sediment production and export to the slope such as observed for the GAB (James & Bone,

2011). The flooding and partial erosion of bioclast-rich coastal dune systems during early sea-level rise likely led to enhanced export of carbonate grains from the shelf to the upper slope. Such now submerged dune systems likely form the ridge that parallels the shelf edge in the current study area (Brook *et al.*, 2014). However, production on the shelf and export to the slope seem to have diminished during interglacial sea-level highstands, leading to more pelagic sedimentation during the interglacials (Fig. 5A and B).

Comparison to the Great Australian Bight

The Eucla Shelf in the central GAB is a warm–temperate carbonate system (James & Bone, 2011), with many similarities to the current study area at the Rottnest Shelf to Carnarvon Ramp transition. However, there are also clear differences in the sedimentary facies between the two regions. The subtropical faunal elements that characterize especially the inner ramp sediments in the study area (zooxanthellate corals, large, warm water, benthic foraminifera, green algae and large gastropods) extend down to 35°S on the Albany Shelf and westernmost part of the GAB (James *et al.*, 1999; James & Bone, 2011). On the Eucla Shelf, in the central part of the GAB, this subtropical fauna was only present during the last major interglacial MIS 5e (James *et al.*, 1999). Sea surface temperatures at IODP Site U1460 were 3 to 5°C cooler during the Middle Pleistocene glacials compared to today (Fig. 5; Petrick *et al.*, 2019). Coral growth therefore would have been limited to small refugia in the present study area during glacials (James *et al.*, 1999), likely further increasing the similarity between the facies on the Eucla Shelf and the study area presented here.

Therefore, it seems unlikely that these differences in facies can explain the apparent different response of the two carbonate platforms to sea-level change. On the contrary, the photozoan elements on the inner ramp of the current study area should rather favour a ‘highstand shedding’ mechanism, which was developed for photozoan dominated tropical platforms. The shelf morphology is another difference between the study area and the Eucla Shelf. The Eucla Shelf has a width of up to 300 km, which is much broader when compared to the Rottnest Shelf or Carnarvon Ramp (Fig. 1). The increase in surface area during transgression is therefore much more pronounced on the Eucla Shelf, potentially contributing to increased shedding of shelfal material to the slope. However, this would not be consistent with other studies that concentrated on Late Pleistocene to Holocene sedimentary processes in the GAB (Boreen & James, 1993; James, 1997; Passlow, 1997; James & Bone, 2011) and New Zealand (Nelson *et al.*, 1982) that made similar observations to those in this study. All of these studies propose that highstand sediments on the upper slope are dominated by pelagic sediments, while resedimented shelf sediments characterize lowstand intervals.

A more likely explanation could be related to changes in the amplitude and duration of glacial to interglacial sea-level changes across the Mid-Pleistocene transition. Saxena & Betzler (2003) and Betzler *et al.* (2005) studied mainly early Pleistocene (Calabrian) intervals from the Eucla Shelf that were deposited before the end of the Mid-Pleistocene transition (MPT), a major transition in global climate that occurred between 1.25 and 0.6 Ma. The MPT is characterized by an intensification of ice ages and a change in the periodicity of the glacial/interglacial cycles from 41 kyr to quasi-100 kyr (Hays *et al.*, 1976). After 0.65 Ma, sea-level reconstructions show an increase in the amplitude of glacial/interglacial variations, with larger glacial sea-level drops of up to 120 m (Bintanja *et al.*, 2005). This coincides with a cooling observed at Site U1460 that likely reflected a weakening of the Leeuwin current due to glacio-eustatic changes (Petrick *et al.*, 2019). After 0.45 Ma, interglacials become warmer with higher sea-levels compared to previous interglacial (Berger & Wefer, 2003). It seems possible that the change in amplitude and duration of glacial–interglacial sea-level variations modified the sedimentological response of temperate carbonate platforms after the MPT (*ca* 0.6 Ma). This seems to have led to a switch from ‘highstand shedding’ dominated systems (Saxena & Betzler, 2003) before to glacial redeposition (Fig. 5, this study; James & Bone, 2011) after the MPT. For the last glacial–interglacial cycle accumulation rates on the upper slope of the Great Australian Bight peaked during the transgression of the late glacial MIS 2 (Hine *et al.*, 2002). This was interpreted as a pulse of increased production and off-shelf transport resulting from initial flooding of the deep shelf (James & Bone, 2011). During continued sea-level rise this re-sedimentation of shelf sediment to the slope diminished towards the Holocene sea-level highstand (Hine *et al.*, 2002; James & Bone, 2011). The lower amplitude glacial to interglacial sea level cycles before the MPT likely resulted in vast shallow water areas on the shelf during interglacial highstands, a situation similar to the initial flooding during the late glacial MIS 2. However, the off-shelf export before the MPT likely persisted during interglacials since the shelf was never as deeply submerged as during the peak flooding of the Middle and Late Pleistocene.

CONCLUSIONS

The Middle Pleistocene to Holocene sequence (last *ca* 430 kyr) at Integrated Ocean Drilling Program (IODP) Site U1460, located at the platform edge to upper slope of the Carnarvon Ramp, contains a record of sea-level controlled sedimentary cycles. Siliciclastic phases are more abundant in the humid interglacials compared to the more arid glacials. Mineralogical differences are also apparent. Feldspar and quartz were deposited during the humid phases, while glacial intervals contain only quartz.

Carbonate sediments deposited during sea-level highstands are fine grained and dominated by grains from a pelagic source with low-Mg calcite (LMC) mineralogy. The lowstand intervals, instead are

coarser-grained, and dominated by grains from benthic organisms with aragonite and high-Mg calcite (HMC) as important mineral phases. During sea-level lowstands and early transgression, the high-energy zone was closer to the shelf edge, leading to winnowing of finer material and redeposition of the coarser, more aragonite-rich and HMC-rich shelfal grains to the location of IODP Site U1460. Partial erosion of calcarenite coastal dune systems during early transgression might have enhanced the export of neritic material from the shelf to the upper slope.

These observations agree with studies from the latest Pleistocene and Holocene of the Great Australian Bight and New Zealand. Results, however, contrast with studies of early Pleistocene (Calabrian) sediments from the Eucla Shelf, in the central Great Australian Bight, indicate that shelfal material was exported to the upper slope during sea-level highstands. It is hypothesized that this difference in sedimentary response is related to the change in duration and amplitude of glacial–interglacial sea-level cycles during the Mid-Pleistocene transition.

ACKNOWLEDGEMENTS

We would like to thank Juan Carlos Laya and an anonymous reviewer for their constructive reviews on our manuscript. Special thanks go to the associate editor Tracy Frank for her constructive and detailed comments on our manuscript. The Integrated Ocean Drilling Program (IODP) is gratefully acknowledged for providing core samples for the study. The authors thank Uwe Wollenberg for his help with XRD measurements and SEM and EDX samples. SEPM is acknowledged for the permission to use parts of figures from James *et al.* (1999) for our Fig. 1. Easy Company is gratefully acknowledged for providing the EasyCore software under an Academic User License agreement. This work was supported by a grant from the German Academic Scholarship Foundation (Studienstiftung des Deutschen Volkes) awarded to Hanaa Deik. Further funding was provided by the DFG (German Science Foundation, Project 320220579) to Lars Reuning.

REFERENCES

- Andres, M.S. and McKenzie, J.A.** (2002) Data report: late Pleistocene oxygen and carbonate isotope stratigraphy in full- and fine-fraction carbonate from the Great Australian Bight, ODP Leg 182, Site 1127. In: *Proceedings of the Ocean Drilling Program* (Eds A.C. Hine, D.A. Feary and M.J. Malone), *Sci. Results*, **182**. Ocean Drilling Program, College Station, TX, 1–13.
- Betzler, C., Saxena, S., Swart, P.K., Isern, A. and James, N.P.** (2005) Cool-water carbonate sedimentology and eustasy; Pleistocene upper slope environments, Great Australian Bight (Site 1127, ODP Leg 182). *Sed. Geol.*, **175**, 169–188.
- Berger, W.H. and Wefer, G.** (2003) On the Dynamics of the Ice Ages: Stage-11 Paradox, Mid-Brunhes Climate Shift, and 100-ky Cycle. In: *Earth's Climate and Orbital Eccentricity: The Marine Isotope Stage 11 Question* (Eds A.W. Droxler, R.Z. Poore and L.H. Burckle). *AGU Geophysical Monograph*, **137**, 41–59.
- Bintanja, R., van de Wal, R.W. and Oerlemans, J.** (2005) Modelled atmospheric temperatures and global sea levels over the past million years. *Nature*, **437**, 125–128.
- Bone, Y., James, N.P. and Kyser, T.K.** (1992) Synsedimentary detrital dolomite in Quaternary cool-water carbonate sediments, Lacedpede shelf, South Australia. *Geology*, **20**, 109–112.
- Boreen, Th.D. and James, N.P.** (1993) Holocene sediment dynamics on a cool-water carbonate shelf; Otway, southeastern Australia. *J. Sed. Res.*, **63**, 574–588.
- Boyer, T.P., Antonov, J.I., Baranova, O.K., Coleman, C., Garcia, H.E., Grodsky, A. Johnson, D.R., Locarnini, R.A., Mishonov, A.V., O'Brien, T.D., Paver, C.R., Reagan, J.R., Seidov, D., Smolyar, I.V. and Zweng, M.M.** (2013). World Ocean Database 2013, NOAA Atlas NESDIS 72, S. Levitus, Ed., A. Mishonov, Technical Ed.; Silver Spring, MD, 209 pp.
- Brooke, B., Creasey, J. and Sexton, M.** (2010) Broad-scale geomorphology and benthic habitats of the Perth coastal plain and Rottnest Shelf, Western Australia, identified in a merged topographic and bathymetric digital relief model. *Int. J. Remote Sens.* **31**, 6223e6237.
- Brooke, B.P., Olley, J.M., Pietsch, T., Playford, P.E., Haines, P.W., Murray-Wallace, C.V. and Woodroffe, C.D.** (2014) Chronology of Quaternary coastal aeolianite deposition and the drowned shorelines of southwestern Western Australia – a reappraisal. *Quat. Sci.Rev.*, **93**, 106–124.
- Collins, L.B.** (1988) Sediments and history of the Rottnest Shelf, southwest Australia: a swell dominated, non-tropical carbonate margin. *Sed. Geol.*, **60**, 15–50.
- Collins, L.B., James, N.P. and Bone, Y.** (2014) Carbonate shelf sediments of the western continental margin of Australia. *Geol. Soc. London, Memoirs*, **41**, 255–272.

Collins, L.B., Zhu, Z.R., Wyrwoll, K.H., Hatcher, B.G., Playford, P.E., Chen, J.H., Eisenhauer, A. and Wasserburg, G.J. (1993) Late Quaternary evolution of coral reefs on a cool-water carbonate margin: The Abrolhos carbonate platforms, southwest Australia. *Mar Geol.* **110**, 203–212.

Courtillat, M. (2019) Reconstruction of oceanographic and atmospheric changes in the Eastern Indian Ocean (NW-Australia, IODP Exp 356) during the Quaternary (Doctoral dissertation). University of Perpignan, Perpignan, France. pp. 287.

Cresswell, G., Boland, F., Peterson, J. and Wells, G. (1989) Continental shelf currents near the Abrolhos Islands, Western Australia. *Mar.Freshw. Res.*, **40**, 113.

Deik, H., Reuning, L., Petrick, B. and Takayanagi, H. (2019) Hardened faecal pellets as a significant component in deep water, subtropical marine environments. *The Depositional Record*, **5**.

Eberli, G.P. (2013) The uncertainties involved in extracting amplitude and frequency of orbitally driven sea-level fluctuations from shallow-water carbonate cycles. *Sedimentology*, **60**, 64–84.

Feary, D., Hine, A.C. and Malone, M. (2000) Great Australian Bight: Cenozoic cool-water carbonates. Proceedings of the Ocean Drilling Program, Initial Reports, College Station, Texas, P. 58.

Gallagher, S.J., Fulthorpe, C.S., Bogus, K., Auer, G., Baranwal, S., Castañeda, I.S., Christensen, B.A., De Vleeschouwer, D., Franco, D.R., Groeneveld, J., Gurnis, M., Haller, C., He, Y., Henderiks, J., Himmler, T., Ishiwa, T., Iwatani, H., Jatiningrum, R.S., Kominz, M.A., Korpany, C.A., Lee, E.Y., Levin, E., Mamo, B.L., McGregor, H.V., McHugh, C.M., Petrick, B.F., Potts, D.C., Rastegar Lari, A., Renema, W., Reuning, L., Takayanagi, H. and Zhang, W. (2017) Site U1460. In: *Indonesian Throughflow* (Eds S. J Gallagher, C. S Fulthorpe and K. Bogus and the Expedition 356 Scientists), proceedings of the International Ocean Discovery Program (vol. 356). College Station, TX: International Ocean Discovery Program. <https://doi.org/10.14379/iodp.proc.356.105.2017>.

Groeneveld, J., Henderiks, J., Renema, W., McHugh, C.M., De Vleeschouwer, D., Christensen, B.A., Fulthorpe, C.S., Reuning, L., Gallagher, S.J., Bogus, K., Auer, G. and Ishiwa, T.(2017) Australian shelf sediments reveal shifts in Miocene Southern Hemisphere westerlies. *Sci. Adv.*, **3** (5), e1602567.

Hallenberger, M., Reuning, L., Gallagher, S.J., Back, S., Ishiwa, T., Christensen, B.A. and Bogus, K. (2019) Increased fluvial runoff terminated inorganic aragonite precipitation on the Northwest Shelf of Australia during the early Holocene. *Sci. Reports*, **9**, 18356.

Hays, J.D., Imbrie, J. and Shackleton, N.J. (1976) Variations in the Earth's Orbit: Pacemaker of the Ice Ages. *Science*, **194**, 1121–1132.

Hine, A.C., Brooks, G.R., Mallinson, D., Brunner, C.A., James, N.P., Feary, D.A., Holbourn, A.E, Drexler, T.M. and Howd, P. (2002) Data report. Late Pleistocene–Holocene sedimentation along the upper

slope of the Great Australian Bight. In: *Proceedings of the Ocean Drilling Program* (Eds A. C. Hine, D.A. Feary, and M.J. Malone), *Sci. Results*, **182**. Ocean Drilling Program, College Station, TX, 1–24.

Hine, A.C., Feary, D.A. and Malone, M.J. (Eds.) (2004) *Proceedings of the Ocean Drilling Program. Sci. Results*, **182**. Ocean Drilling Program, College Station, TX.

James, N.P. (1997) The cool-water carbonate depositional realm. In: *Cool-water carbonates* (Eds N.P. James, and J.A.D Clarke), *SEPM Spec. Publ.*, **56**, 1–20.

James, N.P. and Bone, Y. (2007) A late Pliocene-early Pleistocene, inner-shelf, subtropical, seagrass-dominated carbonate: Roe Calcarenite, Great Australian Bight, Western Australia. *Palaios*, **22**, 343–359.

James, N.P. and Bone, Y. (2011) Neritic carbonate sediments in a temperate realm. Southern Australia, pp. 254. *Springer Science & Business Media*.

James, N.P., Bone, Y., Hageman, S.J., Feary, D. and Gostin, V.A. (1997) Cool-water carbonate sedimentation during the terminal Quaternary-level cycle. Lincoln Shelf, southern Australia. In: *Cool-Water Carbonates: Shelf, Southern Australia* (Eds N.P. James and J.A.D. Clarke), *Spec. Publ. Soc. for Sed. Geol.*, **56**, 53–76.

James, N.P., Boreen, Th.D., Bone, Y. and Feary, D.A. (1994) Holocene carbonate sedimentation on the west Eucla Shelf, Great Australian Bight. A shaved shelf. *Sed. Geol.*, **90**, 161–177.

James, N.P., Collins, L.B., Bone, Y. and Hallock, P. (1999) Subtropical carbonates in a temperate realm. Modern sediments on the southwest Australian shelf. *J. Sed. Res.*, **69**.

Kaczmarek, S.E. and Sibley, D.F. (2011) On the evolution of dolomite stoichiometry and cation order during high-temperature synthesis experiments. An alternative model for the geochemical evolution of natural dolomites. *Sed. Geol.*, **240**, 30–40.

Li, Q., James, N.P., Bone, Y. and McGowran, B. (1999) Palaeoceanographic significance of recent foraminiferal biofacies on the southern shelf of Western Australia; a preliminary study. *Palaeogeogr. Palaeoclimatol. Palaeoecol.*, **147**, 101–120.

Lisiecki, L.E. and Raymo, M.E. (2005) A Pliocene-Pleistocene stack of 57 globally distributed benthic delta O-18 records. *Paleoceanography*, **20**, 17.

Lumsden, D.N. (1979) Discrepancy between thin-section and X-ray estimates of dolomite in limestone. *J. Sed. Res.*, **49**, 429–435.

Nelson, C.S. (1988) An introductory perspective on non-tropical shelf carbonates. *Sed. Geol.*, **60**, 3–12.

Nelson, C.S., Hancock, G.E. and Kamp, P.J.J. (1982) Shelf to basin, temperate skeletal carbonate sediments, Three Kings Plateau, New Zealand. *J. Sed. Res.*, **52**, 717–732.

Nichol, S.L. and Brooke, B.P. (2011) Shelf habitat distribution as a legacy of Late Quaternary marine transgressions: a case study from a tropical carbonate province. *Cont. Shelf Res.*, **31**, 1845–1857.

O'Connell, L.G. and James, N.P. (2015) Composition and genesis of temperate, shallow-marine carbonate muds: Spencer Gulf, South Australia. *J. Sed. Res.*, **85**, 1275–1291.

Pahnke, K., Zahn, R., Elderfield, H. and Schulz, M. (2003) 340000-year centennial-scale marine record of Southern Hemisphere climatic oscillation. *Science* **301**, 948–952

Passlow, V. (1997) Slope sedimentation and shelf to basin sediment transfer. A cool-water carbonate example from the Otway margin, southeastern Australia. In: *Cool-water carbonates* (Eds N.P James, and J.A.D. Clarke), *SEPM Spec. Publ.*, **56**, 107 – 125.

Paul, A., Reijmer, J.J.G., Fürstenauf, J., Kinkel, H. and Betzler, C. (2012) Relationship between Late Pleistocene sea-level variations, carbonate platform morphology and aragonite production (Maldives, Indian Ocean). *Sedimentology*, **59**, 1640–1658.

Pedley, M. and Carannante, G. (2006) Cool-water carbonate ramps. A review. *Geol. Soc. London Spec. Publ.*, **255**, 1–9.

Petrick, B., Martínez-García, A., Auer, G., Reuning, L., Auderset, A., Deik, H., Takayanagi, H., De Vleeschouwer, D., Iryu, Y. and Haug, G.H. (2019) Glacial Indonesian Throughflow weakening across the Mid-Pleistocene Climatic Transition. *Sci. Report*, **9** (1), 1–13.

Puga-Bernabéu, Á. and Betzler, C. (2008) Cyclicity in Pleistocene upper-slope cool-water carbonates. Unravelling sedimentary dynamics in deep-water sediments, Great Australian Bight, ODP Leg 182, Site 1131A. *Sed. Geol.*, **205**, 40–52.

Radwan, O., Bukhamsin, A. and Al-Ramadan, K. (2018) Detrital dolomite. Characterization and characteristics. *Geol. Quarterly*, **62**, 81–89.

Rivers, J.M., Kyser, T.K. and James, N.P. (2009) Isotopic composition of a large photosymbiotic foraminifer. Evidence for hypersaline environments across the Great Australian Bight during the late Pleistocene. *Sed. Geol.*, **213**, 113–120.

Rivers, J.M., Kyser, T.K. and James, N.P. (2012) Salinity reflux and dolomitization of southern Australian slope sediments. The importance of low carbonate saturation levels. *Sedimentology*, **59**, 445–465.

Ryan, D.A., Brooke, B.P., Collins, L.B., Spooner, M.I. and Siwabessy, P.J.W. (2008) Formation, morphology and preservation of high-energy carbonate lithofacies. Evolution of the cool-water Recherche Archipelago inner shelf, south-western Australia. *Sed. Geol.*, **207**, 41–55.

Saxena, S. and Betzler, C. (2003) Genetic sequence stratigraphy of cool water slope carbonates (Pleistocene Eucla Shelf, southern Australia). *Int. J. Earth Sci.*, **92**, 482–493.

Schlager, W., Reijmer, J.J.G. and Droxler, A. (1994) Highstand shedding of carbonate platforms. *J. Sed. Res.*, **64**, 270–281.

Spooner, M.I., De Deckker, P., Barrows, T.T. and Fifield, L.K. (2011) The behaviour of the Leeuwin Current offshore NW Australia during the last five glacial–interglacial cycles. *Glob. Planet. Change*, **75**, 119–132.

Stuut, J.B.W., Temmesfeld, F. and De Deckker, P. (2014) A 550 ka record of aeolian activity near North West Cape, Australia. Inferences from grain-size distributions and bulk chemistry of SE Indian Ocean deep-sea sediments. *Quaternary Science Reviews*, **83**, 83–94.

Swart, P.K. and Melim, L.A. (2000) The Origin of Dolomites in Tertiary Sediments from the Margin of Great Bahama Bank. *J. Sed. Res.*, **70**, 738–748.

FIGURE CAPTIONS

Fig. 1. (A) Location map of Integrated Ocean Drilling Program (IODP) Site U1460, Tamala line (C) and sedimentary facies on the modern seafloor of the Carnarvon Ramp/northern Rottneest Shelf, Australia. Bathymetric contours are in metres (modified after James *et al.*, 1999). Black line marks position of profile shown in (C). (B) Satellite map of western Australia. The white box outlines the study area shown in (A), located between the Carnarvon Ramp and the Rottneest Shelf. (C) Cross-section with distribution of modern facies and location of the IODP Site U1460 (modified after James *et al.*, 1999).

Fig. 2. Lithostratigraphic summary for Integrated Ocean Drilling Program (IODP) Hole U1460A (A) and IODP Hole U1460B (B) (Gallagher *et al.*, 2017). (C) Grain-size fraction >63 μm of sediments from holes A and B (Courtillat, 2019). (D) Siliciclastic (black) versus carbonate (grey) content. (E) Carbonate mineralogy (aragonite, red; high-Mg calcite, yellow; dolomite, blue; low-Mg calcite, green). (F) Integrated stratigraphy based on a comparison between the two alternative age models shown in (G) and (H). (G) Age model from Courtillat (2019) based on $\delta^{18}\text{O}$ *Globigerinoides ruber* (shown), ^{14}C ages and *G. menardii* complex abundance data. (H) Age model from Petrick *et al.* (2019) derived from tuning of the TEX_{86} temperatures to the benthic isotope stack LR04. (I) Sea-level curve calculated from oxygen isotopes (Miller *et al.*, 2011). Note: The time axis applies only for (I).

Fig. 3. Lithostratigraphic summary for Integrated Ocean Drilling Program (IODP) Hole U1460A (A) and IODP Hole U1460B (B) (Gallagher *et al.*, 2017). (C) Grain-size fraction >63 μm of sediments from holes A and B (Courtillat, 2019). (D) Siliciclastic (black) versus carbonate (grey) content. (E) Carbonate mineralogy (aragonite, red; high-Mg calcite, yellow; dolomite, blue; low-Mg calcite, green). (F) Integrated stratigraphy based on a comparison between the two alternative age models shown in Fig. 2. (G) Abundance of bryozoans in one gram of sediment. (H) Abundance of planktic foraminifera in one gram of sediment. (I) Relative abundance of faecal pellets in the fine to medium sand-sized (125 to 500 μm) sediment fraction (Deik *et al.*, 2019).

Fig. 4. Typical sediment textures and component from glacial (A) and (B) and interglacial (C) to (F) deposits. (A) Biogenic sand (>125 μm fraction) and gravel from the glacial isotope stage MIS 8 with abundant bioclasts of bryozoan (br), bivalve (b), worm tubes (w), benthic foraminifera (bf) and scaphopods (s). Echinoderm fragments, which are also common, are not shown in this picture. The sand fraction also contains numerous planktic foraminifera and some ostracods (356-U1460B-4F-2W 62/66). (B) Biogenic sand (>125 μm fraction) and gravel from the glacial isotope stage MIS 10 with abundant bioclasts of

bryozoan (br), bivalve (b), gastropods (g), and worm tubes (w). Azooxanthellate corals (c) are of minor importance (356-U1460B-5F-2W 76/78.5). (C) Thin section photograph (plane polarized light) of a wackestone to packstone from interglacial marine isotope stage 11. Main components are planktic foraminifera (pf) and very fine sand sized unidentified bioclasts. Peloids (p) occur as minor components (356-U1460B-5F-1W 30/34). (D) Biogenic sand (>125 μm fraction) from the interglacial isotope stage MIS 9 consists mainly of planktic and benthic foraminifera (bf). Peloids, echinoderm and bryozoan fragments (not shown) occur as minor components (356-U1460B-4F-3W 37.5/40). (E) Scanning electron microscope (SEM) picture of an ascidian spicule (a), an important aragonite source in the silt fraction (356U1460B-1F-1W-115/119, MIS 1). (F) Dolomite crystals (d) engulf calcite grains (356-U1460B-5F-2W 79/83, MIS 11).

Fig. 5. Conceptual model for the sedimentation during a single sea-level cycle. (A) Interglacial sea-level highstand. Facies zones at the slope to outer ramp/shelf and mud content after James *et al.* (1999) Faunal elements are from James *et al.* (1999) and core analysis from the present study. Mineralogy is derived from the dominant grain types. Skeletal sands are deposited exclusively in the shallowest part of the outer ramp above the storm wave base (James *et al.*, 1999). Most of the slope and outer shelf is dominated by pelagic sedimentation. Sea surface temperatures (SST) are seasonal means from the World Ocean Atlas (Boyer *et al.*, 2013). (B) Glacial sea-level minima, such as during Marine Isotope Stage (MIS) 2. Facies zones are shifted in depth with a sea-level fall of *ca* 120 m. Faunal elements and mineralogy are from the present study's core analysis. Skeletal sands are deposited closer to the position of U1460 resulting in coarser sediments. Pelagic sedimentation is restricted to the slope. Sea surface temperatures (SST) are modern values minus the temperature change reconstructed by Petrick *et al.* (2019). Carbonate grains are produced but not deposited above base of wave abrasion, leading to redeposition to the platform edge and upper slope. (C) At Site U1460 a complete sea-level cycle leads to an alternation between LMC-rich pelagic dominated wackestones and HMC and aragonite-rich, packstones with abundance neritic detritus such as bryozoans and molluscs. HSD, highstand deposits; LSD, lowstand deposits; TSD, transgression deposits.

Table 1. Relative carbonate mineralogy and quartz content depending on the grain size for six samples at the IODP Site U1460. Relative carbonate mineralogy is normalized to a carbonate content of 100%.

Table S1. Mineralogy of sediments at the IODP Site U1460.

Table S2. The MgCO₃ content in HMC and dolomite (mol %) for the studied interval at the IODP Site U1460.

Table S3. Grain size fraction >63 μm for the studied interval at the IODP Site U1460.

Table S4. Bryozoan count for the studied interval at the IODP Site U1460.

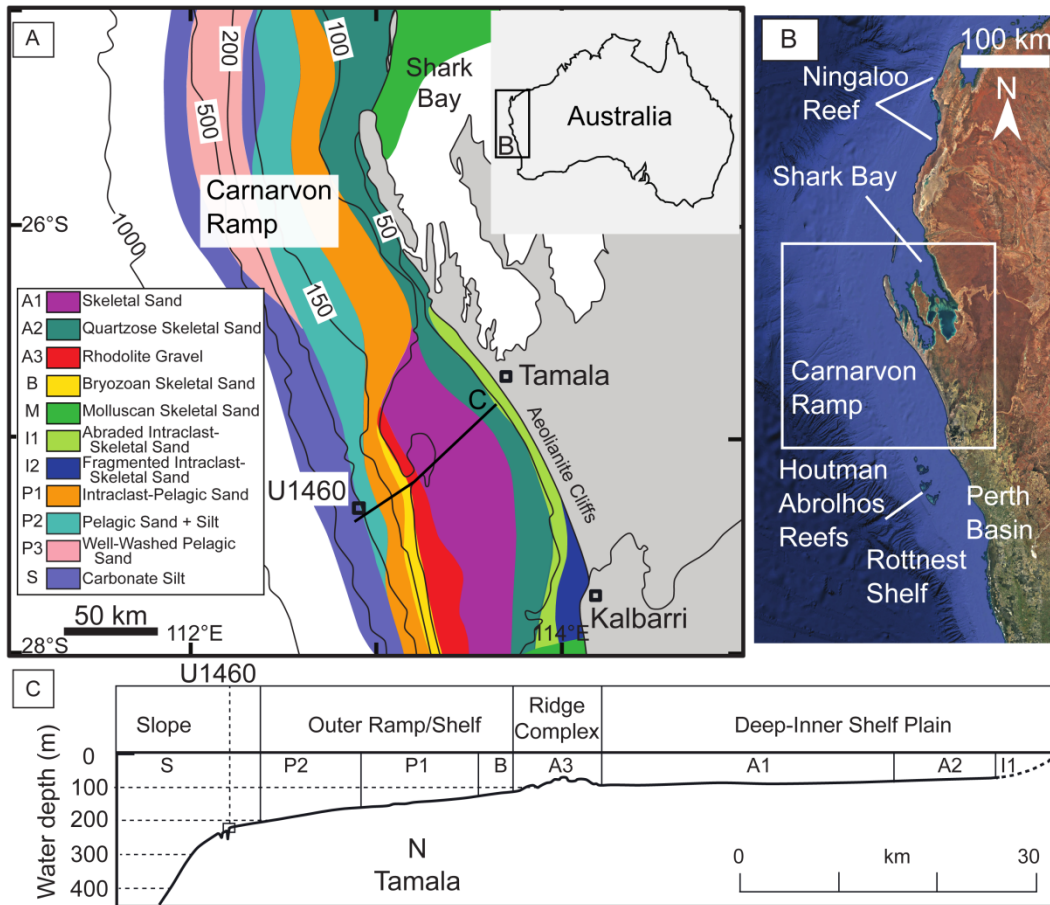
Table S5. Planktic foraminiferal count for the studied interval at the IODP Site U1460.

Table S6. Faecal pellet count for the studied interval at the IODP Site U1460 (Deik *et al.*, 2019).

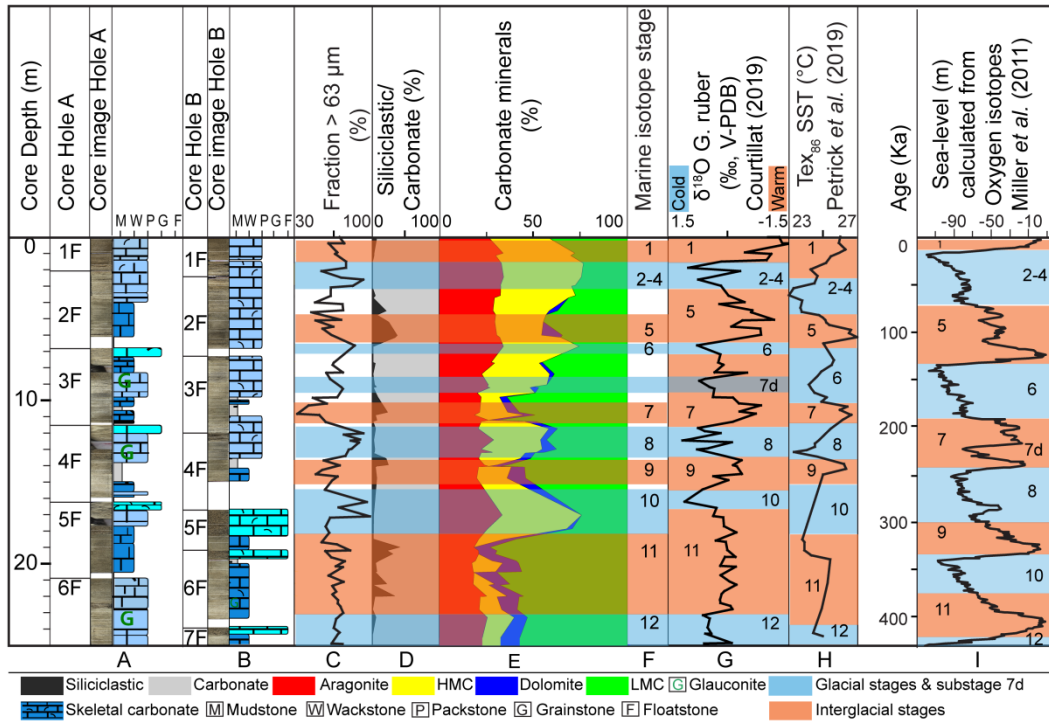
Supplementary information

The dataset is available online in the data repository of this article.

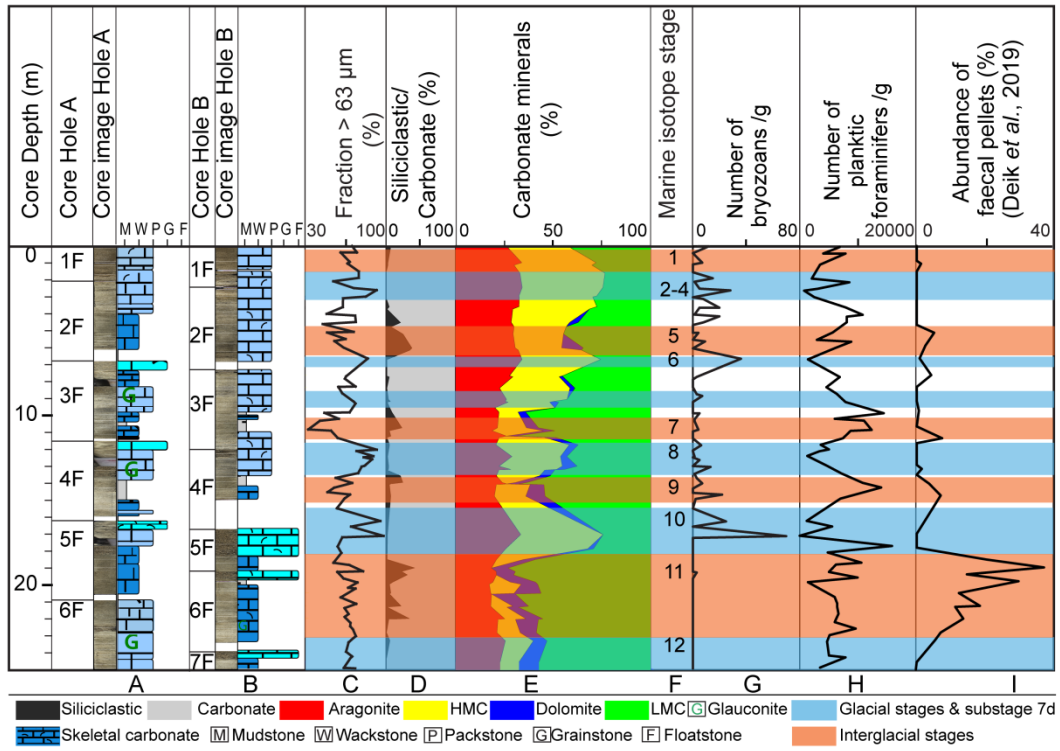
Depth CSF-A (m)	356-U1460B	Grain size	Aragonite (%)	LMC (%)	HMC (%)	Dolomite (%)	Quartz (%)
1.15	1F-1W-115/119	<34 μm	30	37	33	0	5
	1F-1W-115/119	34–63 μm	35	26	39	0	6
	1F-1W-115/119	Bulk	31	29	40	0	3
4.77	2F-2W-67/71	<34 μm	26	46	28	0	3
	2F-2W-67/71	34–36 μm	41	28	30	0	12
	2F-2W-67/71	Bulk	30	43	27	0	7
9.80	3F-2W-100/104	<34 μm	20	66	11	3	5
	3F-2W-100/104	34–63 μm	31	51	15	3	8
	3F-2W-100/104	Bulk	22	64	10	4	8
13.18	4F-2W-62/66	<34 μm	22	56	14	8	2
	4F-2W-62/66	34–63 μm	38	35	22	5	9
	4F-2W-62/66	Bulk	28	44	23	4	4
18.99	5F-2W-79/83	<34 μm	19	65	7	8	2
	5F-2W-79/83	34–63 μm	39	54	11	5	8
	5F-2W-79/83	Bulk	18	73	0	9	5
21.24	6F-2W-54/58	<34 μm	21	64	5	11	2
	6F-2W-54/58	34–63 μm	31	54	9	7	9
	6F-2W-54/58	Bulk	18	63	11	8	3
		<34 μm	23	56	17	5	3
Mean		34–63 μm	34	41	21	3	9



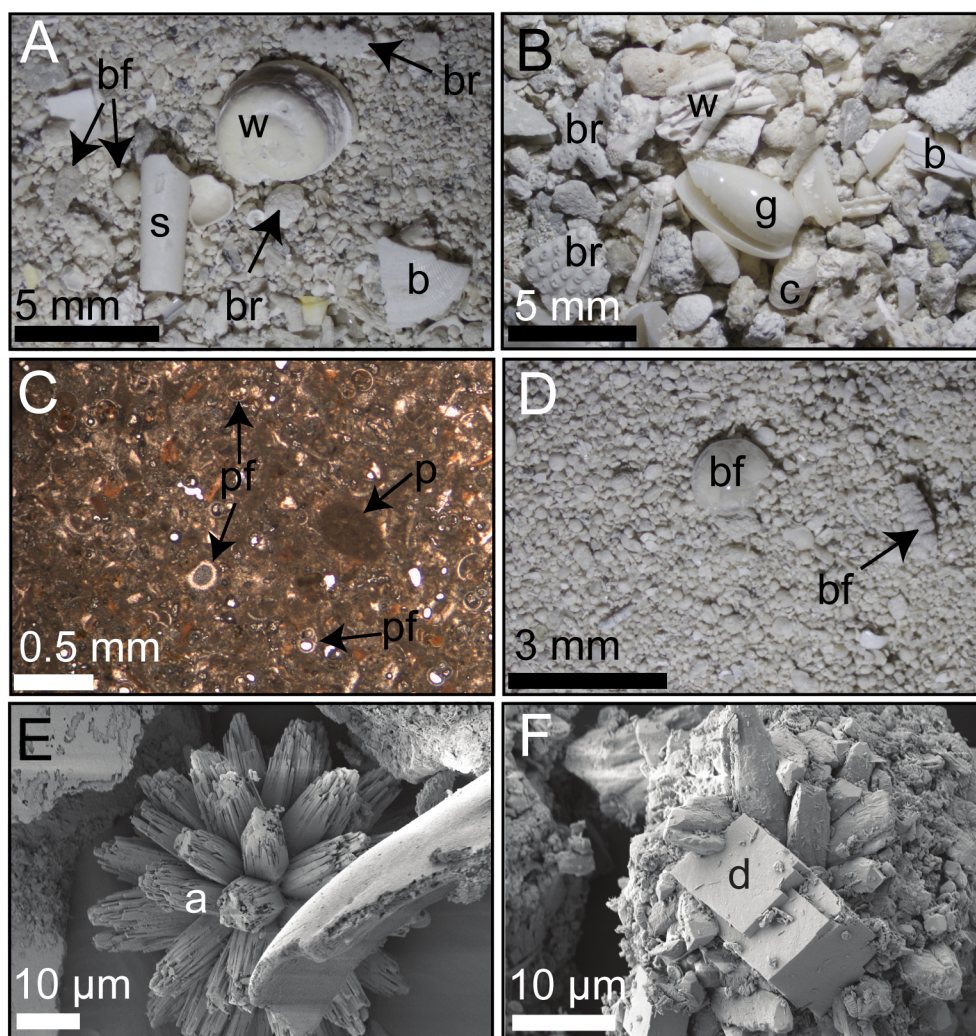
sed_12793_f1.tif



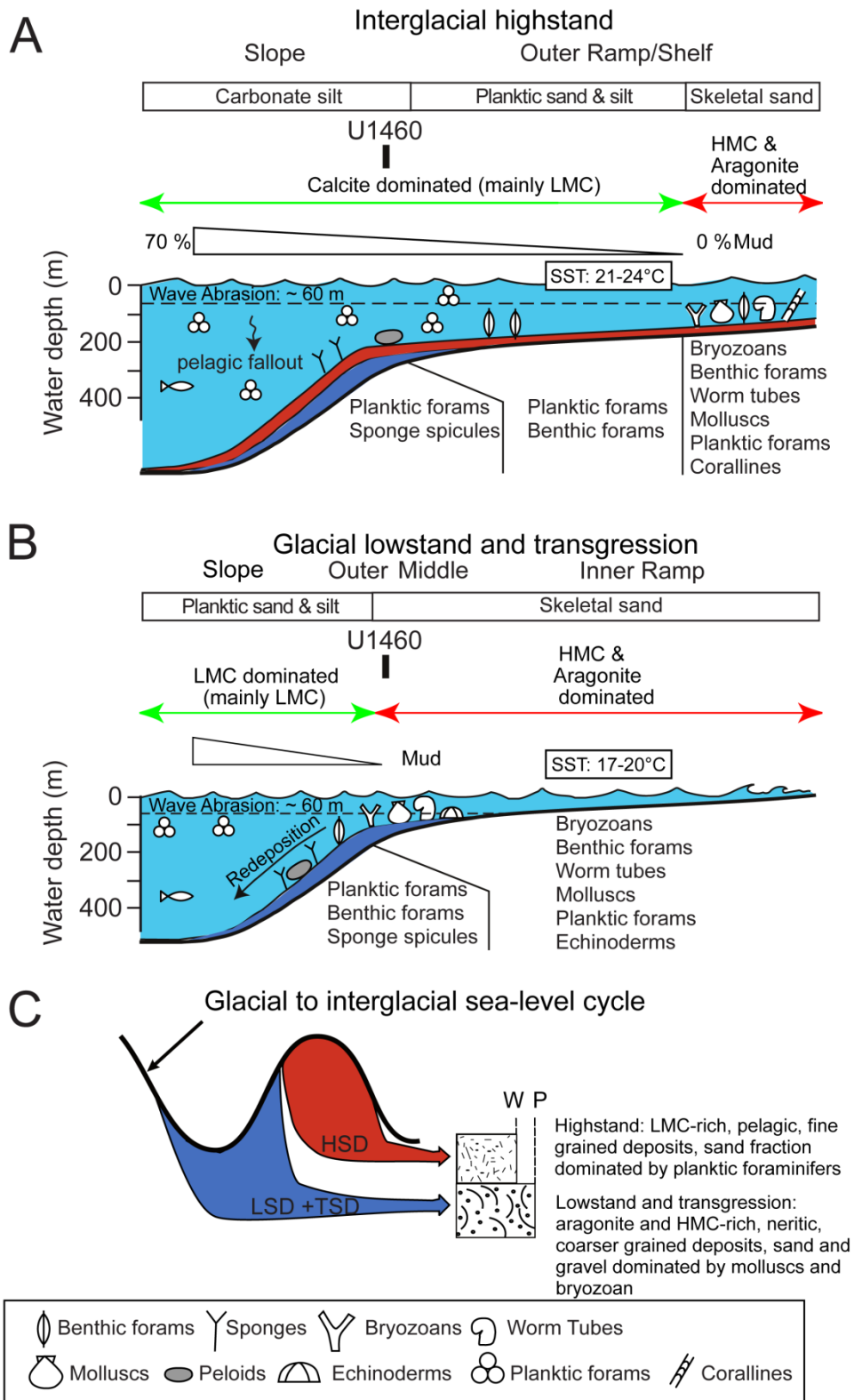
sed_12793_f2.tif



sed_12793_f3.tif



sed_12793_f4.tif



sed_12793_f5.tif